

## RESEARCH ARTICLE

# Robot-based 6D bioprinting for soft tissue biomedical applications

Franziska B. Albrecht<sup>1,2</sup> | Freia F. Schmidt<sup>1</sup> | Christian Schmidt<sup>3</sup> | Rainer Börret<sup>3</sup> |  
Petra J. Kluger<sup>4</sup>

<sup>1</sup>Reutlingen Research Institute, Reutlingen University, Reutlingen, Germany

<sup>2</sup>Faculty of Natural Science, University of Hohenheim, Stuttgart, Germany

<sup>3</sup>Aalen University, Center for Optical Technologies, Aalen, Germany

<sup>4</sup>Faculty of Life Sciences, Reutlingen University, Reutlingen, Germany

## Correspondence

Petra J. Kluger, Faculty of Life Sciences, Reutlingen University, 72762 Reutlingen, Germany as co-first author.

Email:

[petra.kluger@reutlingen-university.de](mailto:petra.kluger@reutlingen-university.de)

Franziska B. Albrecht and Freia F. Schmidt have contributed equally to this study.

## Funding information

Ministry of Science, Research, and Arts Baden Württemberg (IP2019); Paul Hartmann AG

## Abstract

Within this interdisciplinary study, we demonstrate the applicability of a 6D printer for soft tissue engineering models. For this purpose, a special plant was constructed, combining the technical requirements for 6D printing with the biological necessities, especially for soft tissue. Therefore, a commercial 6D robot arm was combined with a sterilizable housing (including a high-efficiency particulate air (HEPA) filter and ultraviolet radiation (UVC) lamps) and a custom-made printhead and printbed. Both components allow cooling and heating, which is desirable for working with viable cells. In addition, a spraying unit was installed that allows the distribution of fine droplets of a liquid. Advanced geometries on uneven or angled surfaces can be created with the use of all six axes. Based on often used bioinks in the field of soft tissue engineering (gellan gum, collagen, and gelatin methacryloyl) with very different material properties, we could demonstrate the flexibility of the printing system. Furthermore, cell-containing constructs using primary human adipose-derived stem cells (ASCs) could be produced in an automated manner. In addition to cell survival, the ability to differentiate along the adipogenic lineage could also be demonstrated as a representative of soft tissue engineering.

## KEYWORDS

6D bioprinting, bioinks, human stem cells, robot arm, soft tissue engineering

## 1 | INTRODUCTION

3D printing of prototypes and components is nowadays an integral part of industrial manufacturing processes [1]. However, in recent years, there has been increasing interest in the use of additive manufacturing for biomedical

applications, with the hope of reproducing more complex geometries in large quantities in the future, bioprinting may also be used to fabricate 3D organs with some functionalities [2, 3]. Today, commercially available 3D bioprinters can realize a simplified layer-by-layer assembly of three-dimensional (3D) tissues [4, 5]. Using different print heads, strands of cell-containing bioinks can be deposited on planar surfaces via a three-axis system on flat planes. These printed constructs can then be cultured and matured into artificial tissues through tissue-specific signals and/or

**Abbreviations:** ASCs, adipose-derived stem cells; DMEM, Dulbecco's modified eagle Medium; GG, gelzan/ gellan gum; LDH, lactate dehydrogenase; MSCGMx, mesenchymal stem cell growth medium; PBS, phosphate-buffered saline.

This is an open access article under the terms of the [Creative Commons Attribution-NonCommercial-NoDerivs](https://creativecommons.org/licenses/by-nc-nd/4.0/) License, which permits use and distribution in any medium, provided the original work is properly cited, the use is non-commercial and no modifications or adaptations are made.

© 2024 The Author(s). *Engineering in Life Sciences* published by Wiley-VCH GmbH.

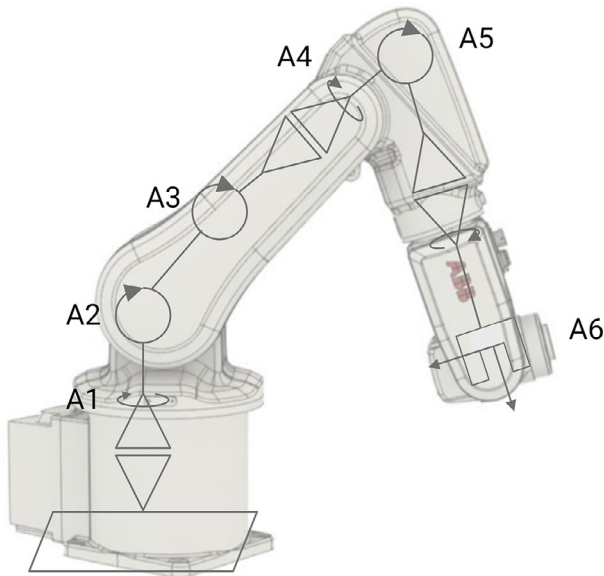


**FIGURE 1** Visualization of the kinematic description of a six-axis robot arm.

mechanical stimuli, and so forth. [6]. Applications include test systems as an alternative to animal testing, their use as clinical tissue substitutes, as well as the production of *in vitro* meat [7, 8]. For this purpose, the further development of numerous materials (e.g., gelatin, alginate) into bioinks, including living human cells, took place [9]. There are multiple 3D bioprinting techniques available, ranging from inkjet-based bioprinting, laser-assisted bioprinting to extrusion-based bioprinting. While inkjet bioprinting requires an almost liquid bioink for processing, and for laser-based systems the materials used must have highly specific properties [10], extrusion-based bioprinting is now favored for biological purposes—even if the construct resolution is limited [11]. It offers the possibility to bioprint a broad range of material viscosities, resulting in the flexible use of multiple materials [12, 13], and further the use of high cell densities [14, 15]. 3D bioprinters available today are very limited in their degrees of freedom of movement. Unsolved challenges are printing of computer-aided design (CAD) models on uneven surfaces (e.g., implants, or in patients), or the production of advanced geometries (e.g., printing in cavities, product rotation during printing, etc.), and simultaneous process and quality control during production [16]. Therefore, the improvement of 3D techniques with regard to the degree of freedom in the printing system is desirable. The advantage of a six-axis system is the use of three rotational (pitch, yaw, roll) and three translational movements ( $X$ ,  $Y$ ,  $Z$ ) and the resulting flexibility, which is illustrated in Figure 1. Thus, each coordinate can be approached from any other point in the print area and the printhead can assume any orientation. For transferring any bioprinting techniques to a six-axis system, the extrusion-based method is the most suitable, since deposit-

### Practical Application

This work demonstrates the successful use of a custom-made bioprinting head for a 6D robot arm for bioprinting viable human stem cells. In addition to the extrusion-driven filament positioning, the printhead has a UV-light diode for crosslinking and a spraying unit to distribute liquids as a fine mist. We were able to show the free-from usage by spraying liquid around a ball. Based on the bioprinting unit and the temperature-controllable printbed, multiple materials with very distinct material characteristics used in soft tissue engineering (collagen, gelatin methacryloyl, and gellan gum) were bio-printed with good print fidelity. Finally, human primary adipose-derived stem cells were bio-printed as an example cell type, and viability and adipogenic differentiation were examined.

ing a continuous filament on uneven and angled surfaces is easier than the targeted positioning of droplets, as is the case with inkjet. The use of laser-based systems should also be avoided, as the 6D applications are intended for *in situ* applications and thus directly on the patient in the long term, where the use of UV light is unsuitable. Especially in the field of personalized medicine, transplants directly on the patient or with complex geometries are of great importance. Here, the technology of 6D bioprinting offers the advantages of printing curved surfaces. Currently, most tissue-engineered soft tissue models are conducted manually, which is problematic in several regards. A manual production process detects quality variances due to individual cell and tissue handling differences. In addition, the demand for models for industrial and academic research makes conventional manual production methods economically inefficient. To overcome these limitations, automation is highly preferable. The implementation of robot systems to conduct all process steps guarantees a reproducible quality of tissue-engineered models. Furthermore, an automated process produces a comprehensive data set of all handling steps that can be analyzed for quality control. Though automated processes have been described for cell culture and the downstream analysis of cell-based assay [17, 18].

Using 3D bioprinting processes in the biomedical field is promising, but innovative development work is still needed to qualify these technologies and devices for future widespread use in the industrial production of biomedical products [19]. Especially in the field of soft tissue engineering, the requirements for automation are high.

The cells to be used are highly sensitive to shear stress and the biomaterial to be used must create a suitable environment for the cells and be printable despite its softness [20, 21]. In addition, it must be possible to reproduce the geometries of large soft tissue defects in order to restore both function and aesthetics to improve the quality of life. To overcome the limitations of 3D printing, there are initial approaches to combine bioprinting with robotic arms that have six degrees of freedom [22].

This study aimed to develop a 6D bioprinting system for biological applications further to develop existing printing and evaluation techniques in soft tissue engineering to realize new biomedical products and quality requirements. To our knowledge, no automated production of soft tissue models by a 6D printing process has been described yet. The result of this highly interdisciplinary approach demonstrates for the first time that it is possible to use a 6D robot arm to deposit viable primary adipose-derived stem cells (ASCs), as precursor cells of the mesodermal germ layer, in pre-designed patterns and thus the construction of soft tissue models. These cells can be differentiated towards adipose tissue, cartilage, and bone [23]. The custom-made 6D bioprinter encompasses a robot arm that can rotate in six axes, offering maximum degrees of freedom. This allows printing in any orientation and on any uneven surface geometry. Thereby the printing nozzle can be positioned at any angle to the surface. In the field of soft tissue engineering and personalized medicine, it is important to produce constructs with a patient-specific geometry to adapt them individually for each patient. We demonstrated the use of all six axes and bioprinting complex geometries with a model ink. To evaluate the suitability of the temperature-controlled self-made bioprinting head, we used biological inks that have completely different material characteristics and find application in soft tissue engineering (gellan gum [GG] [24], collagen [25], and gelatin methacryloyl [26]) and showed high-resolution bioprinting [27]. By cellular bioprinting of primary ASCs and their subsequent differentiation in the adipogenic direction, it could be shown that it is possible to bioprint viable and functional soft tissue-engineered models automatically with our custom-made 6D bioprinting system.

## 2 | MATERIALS AND METHODS

### 2.1 | Custom-made housing for bioprinting

For the intended application, the printer must have sterile working conditions. This could be achieved via the housing which is equipped with a high-efficiency particulate air (HEPA) filter. This filter can be put under

overpressure to achieve a flow to prevent contamination. Further, it encompasses ultraviolet radiation (UVC) lamps for sterilization prior to bioprinting (Figure 2A).

### 2.2 | Custom-made bioprinting unit

The components of the printer are partly commercially available, but the majority are custom-made. In detail, the printing system comprises an ABB IRB 120 industrial robot and a custom-made print head, print bed, and housing.

The robot arm is located in the center of the device. There it is installed on an aluminum plate, positioned in 3D, and performs the movements necessary for printing. The print head is attached via magnets to the robot, containing the (bio)ink while extruding it on the printbed.

The printhead is mechanically connected to the mount by magnets. Centering pins are used to align the printhead so that the print nozzle is located at the tool center point when the printhead is changed. The electrical contact of the printhead is made with the contact surface between the centering pins. This supplies the printhead with power and data. The stepper motor moves the threaded rod and drives the syringe stamp holder. This extrudes the print material from the syringe inserted in the print head. Two optical limit switches are installed to move the extruder axis to the zero point.

To enable different temperatures while printing a Peltier element is included. This is supplied electronically via the contacts on the back and underside of the print head. The thermal heat generated during the temperature control of the syringe is removed via the heat sink with the use of a fan.

The crosslinking module can perform ionic and photo-based crosslinking. The module is installed between the robot flange and the printhead holder and includes two ultraviolet (UV) light emitting diodes (LEDs) with wavelengths of 365 and 405 nm and a spray head that can diffuse fluids. Inside the housing, there is an airbrush system for this process. This is operated using external compressed air or sterile medical gas and finely spraying the material. The crosslinking solution is fed into the airbrush gun via a liquid reservoir. To regulate the amount of crosslinking solution that is sprayed, a servo motor is used to actuate the trigger of the airbrush gun. Furthermore, changing the air pressure can regulate the amount of material sprayed.

The entire print bed is placed directly on the 30 mm thick aluminum robot plate. To eliminate the heat sink for the Peltier element, it is placed directly on the robot plate and thermally coupled with a heat-conducting paste. This makes the robot plate a cooling surface for the Peltier element, which can be used to remove the waste heat. The cooled metal surface of the print bed is placed on the Peltier element and thermally coupled with heat-

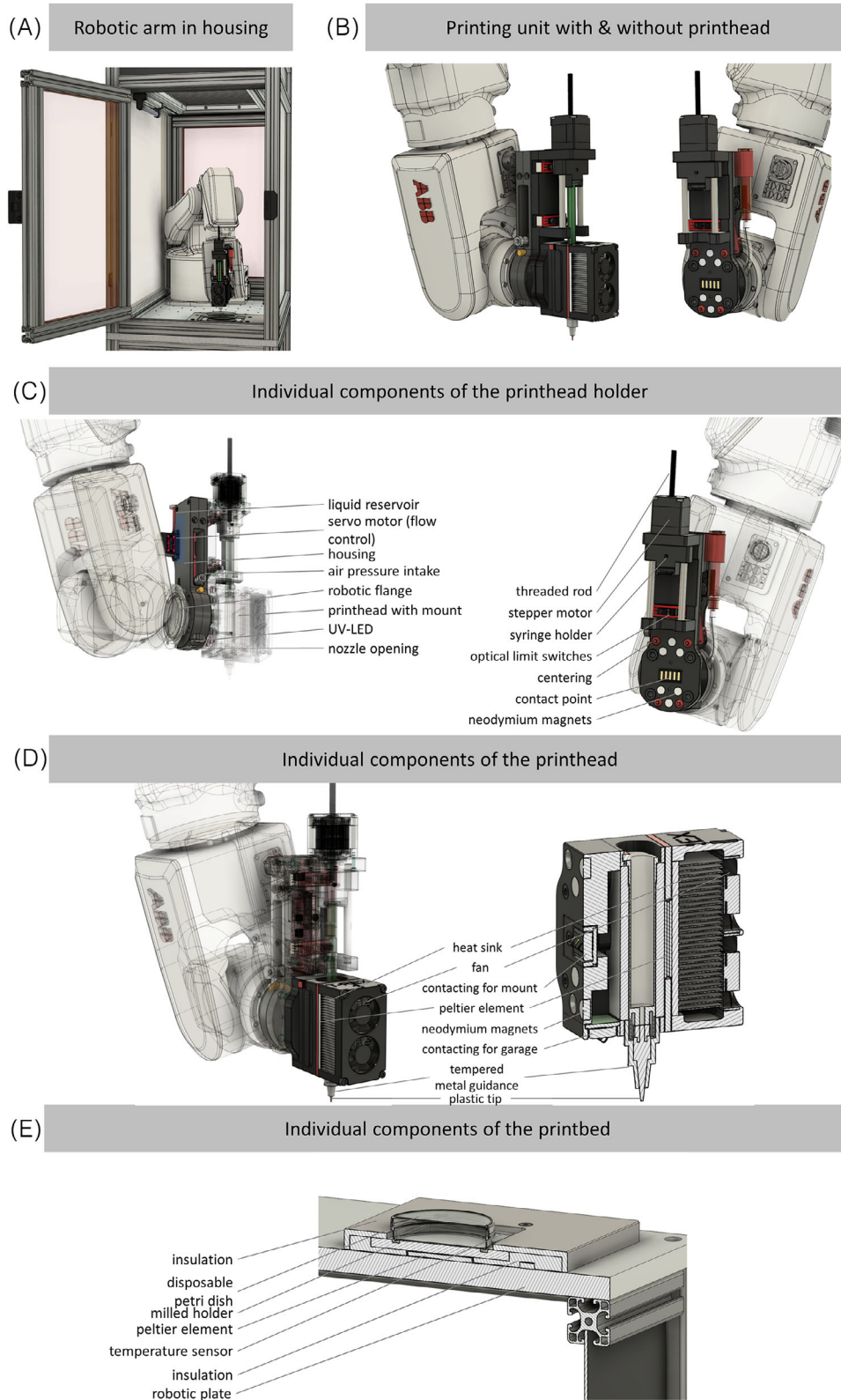


**FIGURE 2** Schematic illustration of self-made printing parts. (A) Robot arm in the surrounding housing. (B) Printing unit attached to the robot arm with and without printhead. Detailed presentation of the individual components of the printhead holder (C), the printhead (D), and printed bed (E).

**TABLE 1** Bioprinting parameters for all used model inks.

	Model ink	GG	Collagen	GM2A8
Nozzle diameter (μm)	410	410	410	410
Velocity (mm/s)	10	10	10	10
Temperature print head (°C)	35	28	8	20
Temperature print bed (°C)	15	8	38	8
Crosslinking	Decreased T (°C)	Ca <sup>2+</sup> ions	Increased T (°C)	UV-light

Abbreviation: GG, gellan gum.

conducting paste. This is made of a 5 mm thick aluminum plate equipped with a milled contour. This milling contour is designed to fit a petri dish in which the printed object is produced. In addition, this metal plate has lateral holes in which temperature sensors are incorporated. An insulation part is placed to separate the heated robot plate from the cooled metal surface. To improve the thermal connection between the cooled metal surface, Peltier element, and robot plate, the metal surface and Peltier element are screwed onto the robot plate using the plastic cover and four screws. The screw connection presses the package of the robot plate, Peltier element, and cooled metal surface together with force, which improves the thermal connection.

### 2.3 | Viscosity measurement

Viscosity was determined with a RheoStress 1 (Thermo Scientific). The cone (C35/1) was rotated for 30 s in the material before a 30 s break followed before measurement. For measurement, the cone was lowered onto the carrier plate and rotated with a preset shear rate of 50 s<sup>-1</sup> while the carrier plate increased temperature from 10 to 40°C (1°C steps).

### 2.4 | Acellular bioprinting

More complex models (nose and ear) were bioprinted with NIVEA Crème as model ink (Beiersdorf AG). Acellular grid models were made with a self-made GG ink (details see bioink formulation), a collagen ink (Lifeink 200, CellSystems), and a gelatin methacryloyl-acetyl ink (GM2A8, Fraunhofer IGB). The desired grid was set to 20 mm × 20 mm with a bar dimension of 0.67 mm and inner grids with an edge length of 4 mm × 4 mm. The used parameters are depicted in Table 1.

## 2.5 | Human samples

Patients gave their written agreement to donate the samples. All research was carried out according to the declaration of Helsinki, defining rules for the work with human beings, and according to the permission of the Landesärztekammer Baden-Württemberg (F-2012-078).

### 2.5.1 | Cell isolation and culture

Primary human ASCs were isolated as published elsewhere. Briefly summarized, adipose tissue was cut into 5 mm pieces and incubated with the same volume of collagenase solution (100 U/mL collagenase (Serva) in Dulbecco's Modified Eagle Medium [DMEM, Pan Biotech] with 1% bovine serum albumin (Biomol)) for 3 h at 37°C under mild agitation. Afterward, the suspension was filtered twice (first through 500 μm, second through 200 μm mesh), and the filtrate was centrifuged. The incubation of the resulting cell pellet in erythrocyte lysis buffer (155 mm ammonium chloride, 0.1 mm ethylenediaminetetraacetic acid) for 10 min followed. After another centrifugation step, the pellet was resuspended in phosphate-buffered saline (PBS, Lonza), filtered through a 70 μm strainer (Greiner BioOne), and centrifuged again. Finally, the aspiration of the supernatant and the resuspension of the pellet in Mesenchymal Stem Cell Growth Medium (MSCGMx, PeloBiotech) took place.

Cells were seeded with an initial cell density of 1 × 10<sup>6</sup>/25 cm<sup>2</sup> in MSCGMx and were used until passage four.

### 2.6 | Cell-containing bioink formulation

For the bioink, 150 mg GG (Gelzan, Sigma Aldrich) was dissolved in 9 mL aqua bidest., heated until boiling, and tempered at 37°C.

Cells were trypsinized (0.05% trypsin-EDTA (Gibco) in Versene (Lonza)), and cell density was adjusted to 1.5 × 10<sup>6</sup> cells per 100 μL MSCGMx. The final bioink mixture contained 900 μL GG-solution with 100 μL cell suspension gently mixed by pipetting up and down with a 1 mL syringe (Braun Melsung).

#### 2.6.1 | Manual model generation

For manual models, 100 μL cell-containing bioink was extruded manually into a house-made mold (9 mm diameter) with a 1 mL syringe. The crosslinking with 1 mL PBS

followed immediately. After 30 min, the mold and PBS were removed, and 1 mL fresh differentiation medium was added.

## 2.6.2 | Additive model generation

Additive models were bioprinted with the self-made printhead and the 6D robot arm (ABB IRB 120). After filling the 1 mL syringe with cell-containing bioink, the bioink was transferred into a 3 mL syringe and placed in the printhead. Selected parameters (see Table 1). As a sterile printbed, a single-use petri dish with 9 cm diameter was used. After printing, models were rinsed with 1 mL PBS and left for the gelation process for 30 min. Placing the models into a 24-well plate (Greiner BioOne) with 1 mL differentiation medium followed immediately.

## 2.7 | Culture conditions

All models were cultured in 1 mL of differentiation medium, which was changed in half three times a week. Differentiation medium contained DMEM supplemented with 10% fetal calf serum (Pan Biotech), 1% penicillin/streptomycin (Lonza), 870 g/L stable glutamine (Pan Biotech), 500  $\mu\text{m}$  3-Isobutyl-1-methylxanthine, 100  $\mu\text{m}$  indomethacin, 1  $\mu\text{g}/\text{mL}$  insulin, and 1  $\mu\text{m}$  dexamethasone (all Sigma Aldrich)

## 2.8 | Live-dead staining

According to the manufacturer's instructions, the live-dead staining was performed (live-dead staining kit for mammalian cells, Invitrogen). Briefly, the models were given in 1 mL PBS with 0.5  $\mu\text{L}$  calcein, 2  $\mu\text{L}$  Ethidium homodimer, and 1  $\mu\text{L}$  Hoechst 33,342 (Cell Signaling) for 60 min. Microscopy took place at an Axio Observer microscope with an AxioCam 305 (color camera) using ZENblue software (all Carl Zeiss).

## 2.9 | Lactate dehydrogenase (LDH) assay

For LDH determination, a commercially available kit (Takara Bio) was used. Phenol red-free, conditioned medium was created (24 h) and used as samples. Color development took place by adding 50  $\mu\text{L}$  LDH reagent (1 catalysator: 50 dye) to a triplicate of 50  $\mu\text{L}$  sample. Absorbance measurement followed after 30 min incubation at a wavelength of 490 nm and a reference set at 680 nm.

## 2.10 | Resazurin assay

For resazurin development, phenol red-free cell culture medium was supplemented with 0.11  $\mu\text{g}/\text{mL}$  resazurin (Sigma Aldrich) and incubated with the cells for 24 h. The occurred absorbance of 100  $\mu\text{L}$  triplicates was measured at a wavelength of 570 nm with a reference at 600 nm.

## 2.11 | Lipid and cytoskeleton staining

Prior to staining, hydrogels were fixated for 3 h in Histofix (Carl Roth) and washed overnight with PBS. The staining solution contained 1  $\mu\text{g}/\text{mL}$  BodiPY 493/503 (Cayman Chemicals), Hoechst 33,342, and two droplets of ActinRed 555 (Invitrogen). Samples were left for 1 h in the staining solution and after washing twice with PBS microscopied.

## 3 | RESULTS AND DISCUSSION

This project aimed to develop a custom-made bioprinting tool for a 6D robot arm usable for soft tissue engineering applications.

### 3.1 | Custom design of the 6D bio-printer

The overall structure and layout of the 6D bio-printer have been precisely adapted to the needs of applications in soft tissue engineering applications. A schematic overview of the custom-made bioprinting system is shown in Figure 2.

Due to the surrounding housing (Figure 2A) with an included HEPA filter, the robot arm was optimized for sterile bioprinting, which is generally required for working with living cells. It prevents the printing environment from coming into contact with the room air and, therefore, with possible contaminants or airflow. The magnets on the printing unit allow for a quick exchange of the printhead (Figure 2B,C), while the UV lamp makes crosslinking of materials possible. The other components (e.g., threaded rod, stepper motor, contact point) are responsible for controlling the extruded filament and the movement in general. Also included here is the liquid reservoir to spray fluids like cell culture medium or crosslinking solutions as a fine mist.

The printhead has a complex and detailed setup, as demonstrated in Figure 2D. Multiple components are included, allowing for bioprinting of different biological materials used in soft tissue engineering like GG [24], collagen [25], and gelatin methacryloyl [26]. This wide-ranging material processing is achieved not least through the individual components of the printhead, which are

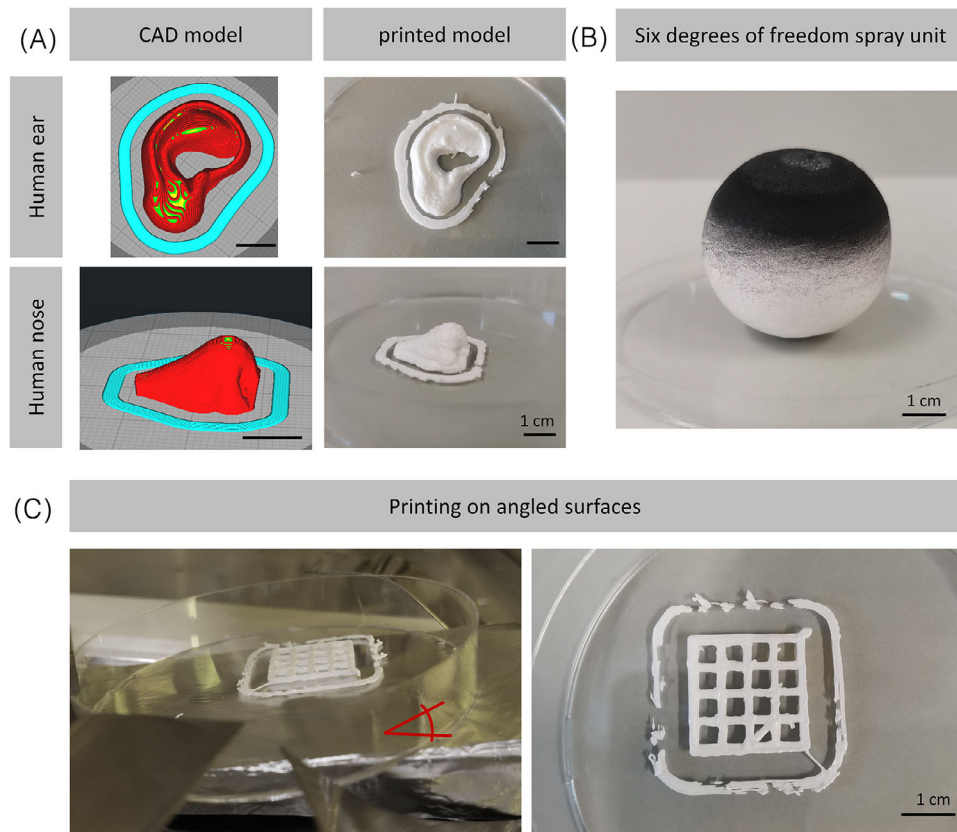


**FIGURE 3** Possibilities of the flexibly deployable robot arm. (A) CAD model and 3D printed complex structures with a model ink. (B) sprayed ball using the six degrees of freedom spraying unit. (C) 3D bioprinting on a printing surface angled at  $10^\circ$  and finished model. Scale bar 1 cm.

displayed in 3D. The installed components enable a temperature-controllable printhead, which in turn positively affecting cell viability. As for bioprinting, the bioinks and the encapsulated cells must maintain a specific and selectable temperature, multiple components were installed to enable a temperature-controllable print head. Similar holds for the printbed, for which the temperature can also be adjusted (compare Figure 2E). The flexible heating and cooling helps to achieve a higher printing resolution, as the deposited filament of the (bio)ink reaches the set temperature (e.g., necessary for crosslinking) quicker.

### 3.2 | The extension of a 6D robot arm fulfills all important requirements for a 6D bioprinter

Especially for biomedical purposes, it is crucial that a bioprinter is able to follow closely successive points of the provided CAD file. As this enables to rebuild the model with rounded and not square edges resulting in better comparability. More complex CAD models in the form of a nose and ear were printed (Figure 3A) with the model ink to ver-

ify this capability [28, 29]. Comparing the respective model with the CAD template, it is evident that there is a remarkable similarity. The individual layers with deepening and targeted pores are visible in both models, suggesting an adequate synchronization of robot motion and extrusion. The small material overhangs on the exposed edges are due to the material used and not to improper extrusion. Due to the high viscosity and stability of the model ink, a small amount of the extruded material adheres to the nozzle and is thus easily pulled along. Appropriate synchronization between the motion and the extrusion is a necessary condition for any 3D printer. However, more requirements must be tested to create a system with six degrees of freedom. These are shown in Figure 3B,C. The results of a sprayed cotton ball can be seen in part B. By spraying the upper half of the sphere, it can be shown that not only the spatial position of the print head but also its orientation can be controlled. As a result, the color is evenly distributed over the entire area, which allows the conclusion that the installed brush system is permanently positioned perpendicular to the spherical surface. This ability is a fundamental prerequisite for printing with six degrees of freedom. Since the nozzle is located at the lower part of the

print head, completely spraying the sphere was impossible, as the robot arm for the lower half would have collided with the housing.

Last, the possibility of printing on angled surfaces was tested. This is also impossible with a commercial 3D bioprinter but offers decisive freedom for biomedical applications. As can be seen (Figure 3C), the entire print bed was changed to an angle of  $10^\circ$  while maintaining a straight print surface. Here, too, the capability of parallel alignment of the print head to each print point on the print bed is utilized. The printed grid structure shows no distortion due to the angled surface, indicating a well-adjusted central control unit. This is also confirmed by the high resolution of the printed grid without any wiggly edges.

In summary, the results demonstrate that the custom-made 6D bioprinter fulfills all crucial requirements for bioprinting in six dimensions. The robot movement and material extrusion are highly synchronized, and the print head (with extrusion and spray unit) can be permanently aligned perpendicular to the surface.

### 3.3 | Using different biological inks enables the use in diverse application areas

The more different materials a bioprinter can process, the more flexible the application areas can be designed. Especially for biomedical applications, it is advantageous because different tissues can be manufactured with the same device. Three materials that vary widely in terms of material properties were processed to demonstrate the diversity of the built print head unit. The materials GG (bacterial exopolysaccharide), modified gelatin (with acetyl and methacrylic groups), and collagen were used as examples of inks. The printed grids (A), their accuracy (B) compared to the CAD file, and the determined viscosity (C) are depicted in Figure 4. Before the bioprinting tests, printing parameters were tested and adjusted for each material individually. Closely examining the printed grid structures reveals that the desired shape could be printed with all three materials. However, they differ in their resolution and, thus, in their accuracy.

The deviation in the accuracy of the individual models is due to the specific material properties and not to the printhead. Starting with GG, the approximately 180% wider inner bar can be explained by the initial lack of ionic crosslinking and the slowly decreasing temperature. The weight of the upper layers' presses on the not yet fully crosslinked lower layers, causing them to spread. If the outer bar is considered, the deviation is small at around 6%, but slight unevenness can be seen. The viscosity of the ink can explain all the phenomena described. Over  $\sim 34^\circ\text{C}$ , the

GG ink exhibits low viscosity flow behavior, below  $34^\circ\text{C}$  the viscosity increases sharply. This explains why the ink has to be printed at  $38^\circ\text{C}$  and then cooled down as quickly as possible to generate stable constructs. However, due to the higher viscosity during extrusion, GG is less flowable, which means that the surface tension has little influence on smoothing the extruded filament.

The collagen ink shows the slightest percentage deviations from the CAD model with a 0.5% decreased outer bar and a 65% increased inner bar. Here, too, the viscosity measurement allows conclusions to be drawn about the results because collagen has a high viscosity at the printing temperature of  $10^\circ\text{C}$ , preventing the ink from spreading. Furthermore, the increase in temperature of the print bed further increases the viscosity of the ink resulting in an accurate model geometry.

Last, the gelatin-based ink was evaluated. It is obvious that the grid structure itself shows good resolution with smooth outer and inner bars, which are increased by 4% or 125%, respectively. Again, viscosity helps explain these results. Based on the printing temperature, the material shows a more or less fluid behavior (above  $15^\circ\text{C}$ ) during extrusion. This causes the material to flow after deposition despite a cooled print bed because the viscosity does not increase until below a temperature of about  $16^\circ\text{C}$ , which presumably did not happen fast enough. At the same time, the surface tension inside the liquid ink explains the smooth edges of the grid, which can be retained after cooling down and crosslinking via ultraviolet light.

Regardless of the accuracy of the printed grids with the model inks used, it was possible to show that the self-made print head can be used very flexibly for a wide variety of materials. It was possible to precisely maintain set temperatures over a longer time, thus enabling the materials to be extruded. This flexibility of the print head, in combination with the crosslinking by UV light or sprayed fluids and the temperature-controllable print bed, extends the material range. Material-related inaccuracies of the models could be reduced by further adjustments of the parameters or adapted slicing conditions.

### 3.4 | The comparability of automatically with manually produced cellular hydrogels demonstrates the applicability of the printer

Automated production of biological constructs by bioprinting may negatively affect cells, for example, due to the pressure applied or the production time. [30] As a biological model, ASCs were printed in GG. Cell viability, metabolic activity, and the ability to differentiate were

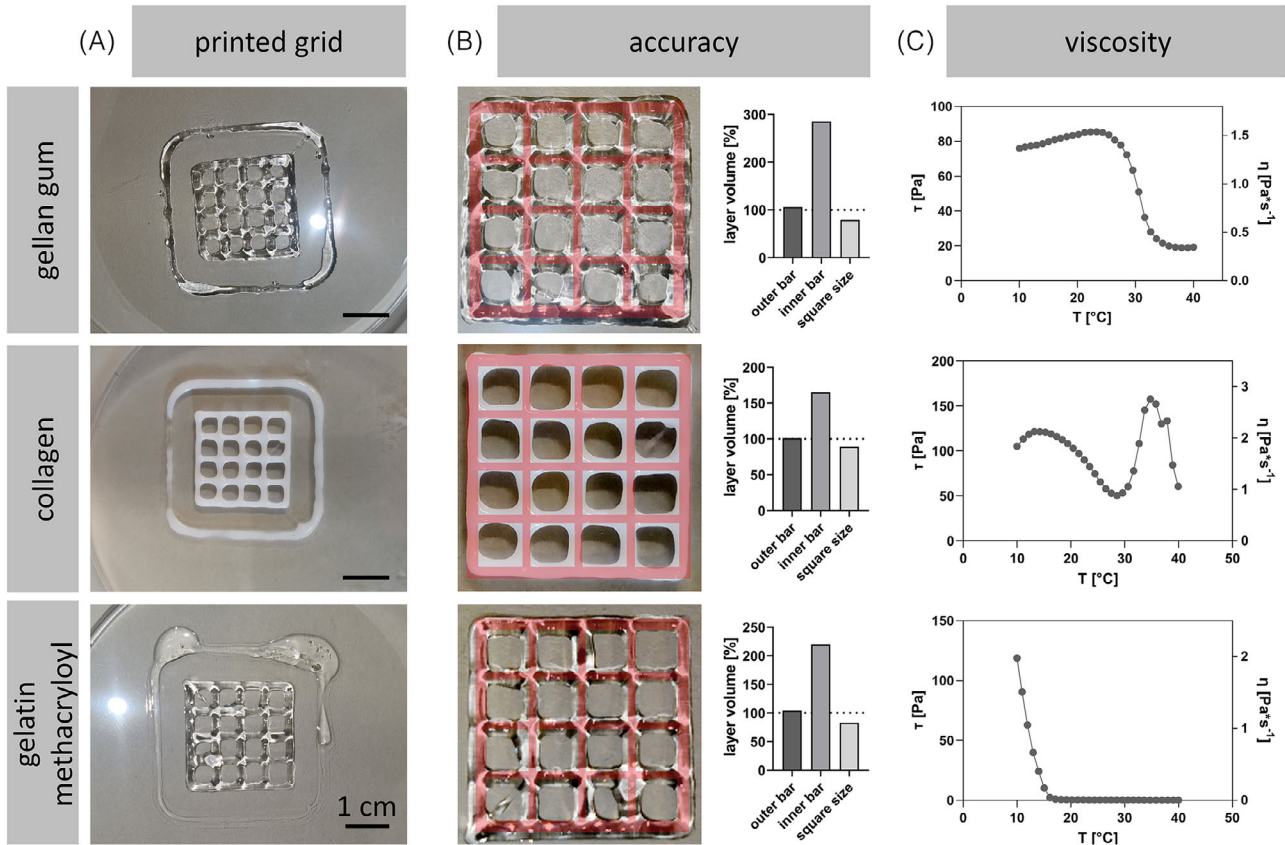


**FIGURE 4** Demonstration of the flexibility of the built printhead using different model inks, GG, collagen, and gelatin methacryloyl. Printed grid structure (A), analyzed accuracy (B), and determined viscosity (C) from left to right. GG, gellan gum.

determined to evaluate the equivalence of the automatically produced cellular hydrogels to hydrogels that were generated manually (Figure 5).

Cell viability was assessed by live-dead staining and quantitatively by LDH assay on days 1, 8, and 15 (Figure 5A). It showed few dead cells in the live-dead for both production modes and no difference either on the culture days or for the production mode. Quantitative determination showed an increased LDH release on day 1 of culture compared to day 8 or day 15, nevertheless, independent of the preparation (Figure 5B).

The metabolic activity of the cells in the hydrogels was determined by a resazurin assay which showed no significant difference between the preparation methods (Figure 5B). During culture and differentiation, the metabolic activity of the cells decreased slightly compared to day 1.

It is well known that ASCs can be differentiated along the mesodermal germ layer. [23] The ability to differentiate was assessed by adding factors that have been shown to lead to adipogenic differentiation of ASCs over 15 days. Immunofluorescence staining of the actin cytoskeleton and of the incorporated lipids was performed (Figure 5C).

Studies have already shown that not adjusted printing conditions have an impact on the viability and integrity of stem cells. [31] In our approach, we detected similar viability and differentiation for ASCs in manually and additively fabricated models. Hence, the printing conditions of our 6D printer are suitable for soft tissue generation.

#### 4 | CONCLUDING REMARKS

Taken together the results of this study demonstrate that this 6D robot printing system is a promising tool for the automated production of complex tissue models and creates an important prerequisite for the applicability in personalized medicine in the future. The advantages of 6D printing lie in the expansion of the possibilities and areas of application. It is possible to print on uneven surfaces and to adapt the geometry to the extent that it can be printed directly on the patient. In addition, manufactured transplants will be completely free to adapt to the shape of the defect. With a few adjustments, the printer can be expanded for a variety of other applications in the field of in vitro models or even in situ

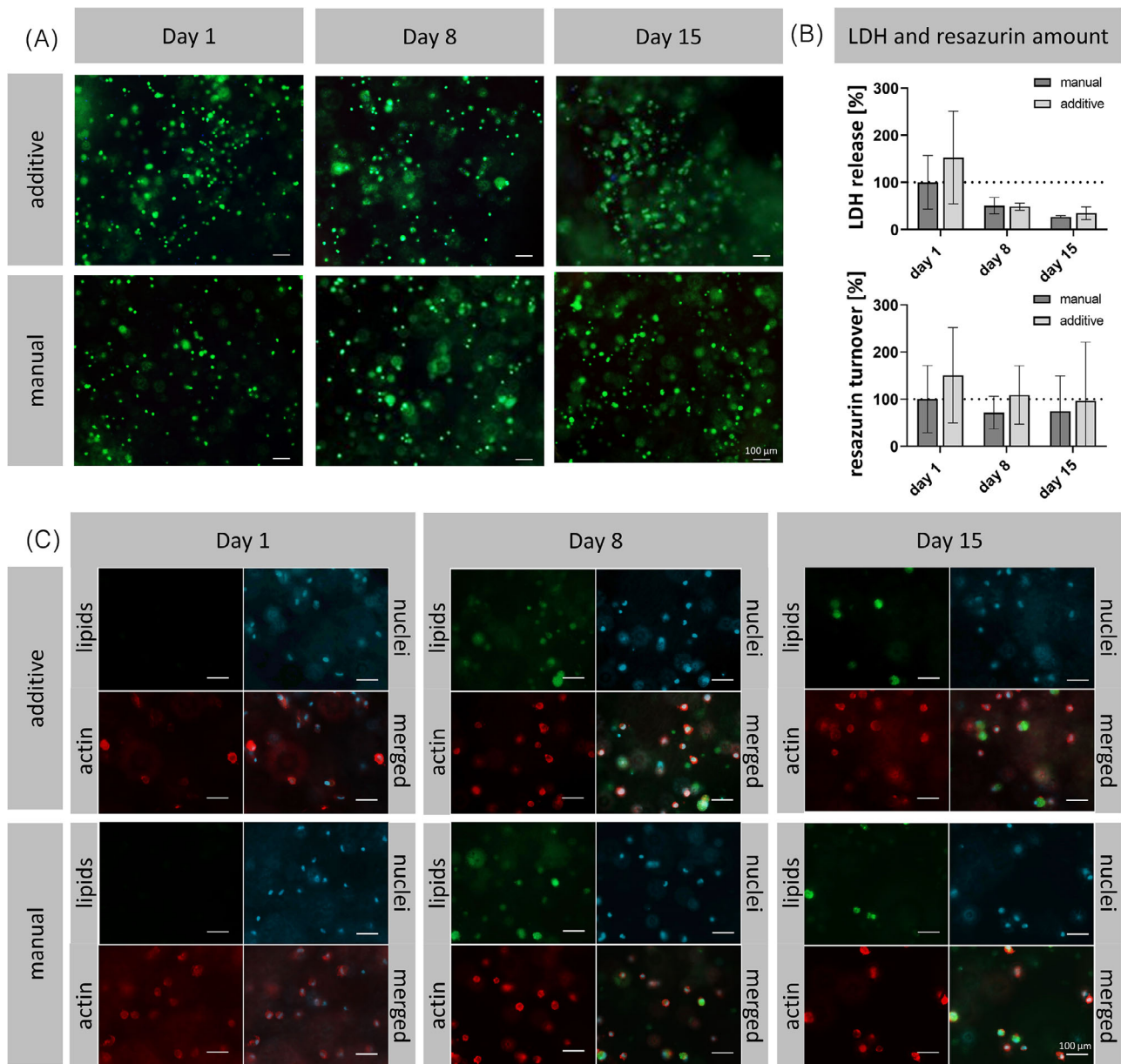


**FIGURE 5** Cell viability and function after bioprinting and manual setup on days 1, 8, and 15. (A) live-dead staining of cellular hydrogels. Viable cells are shown in green, dead in red, and cell nuclei in blue, scale bar 100  $\mu\text{m}$ . (B) quantitative determination of LDH release and resazurin turnover. Values are depicted as mean  $\pm$  standard deviation. (C) co-staining of intracellular lipids, actin cytoskeleton, and cell nuclei. Scale bar 100  $\mu\text{m}$ . LDH, lactate dehydrogenase.

bioprinting, thus enabling it to be used in various fields of biomedicine.

#### AUTHOR CONTRIBUTIONS

Conceptualization, Franziska B. Albrecht, Freia F. Schmidt, Rainer Börret, Petra J. Kluger; Methodology, Franziska B. Albrecht, Christian Schmidt; Formal analysis, Franziska B. Albrecht, Christian Schmidt; Investigation, Franziska B. Albrecht; Christian Schmidt; Validation, Franziska B. Albrecht, Freia F. Schmidt; Visualization, Franziska B. Albrecht, Freia F. Schmidt;

Writing—Original Draft, Franziska B. Albrecht, Freia F. Schmidt, Christian Schmidt; Writing—Review and Editing, all authors; Funding Acquisition, Freia F. Schmidt, Rainer Börret, Petra J. Kluger; Resources, Petra J. Kluger; Supervision, Freia F. Schmidt, Petra J. Kluger.

#### ACKNOWLEDGMENTS

The authors thank Dr. Ziegler and Team (Klinik Charlotenhäuser, Stuttgart, Germany) for kindly providing the human adipose tissue and skin samples from elective surgery. Furthermore, we are grateful for the financial sup-

port of the Ministry of Science, Research, and Arts Baden Württemberg (IP2019) and the Paul Hartmann AG.

## DATA AVAILABILITY STATEMENT

The data that support the findings of this study are available from the corresponding author upon reasonable request.

## ETHICAL APPROVAL

The patients gave their written consent to donate the biopsies. All research was conducted in accordance with the Declaration of Helsinki, which lays down rules for work on human subjects, and with the approval of the Landesärztekammer Baden-Württemberg (F-2012-078).

## REFERENCES

- Hao B, Lin G. 3D Printing technology and its application in industrial manufacturing. *IOP Conf Ser: Mater Sci Eng.* 2020;782:022065.
- Gu Z, Fu J, Lin H, He Y. Development of 3D bioprinting: from printing methods to biomedical applications. *Asian J Pharm Sci.* 2020;15(5):529-557.
- Ng WL, Chua CK, Shen Y-F. Print me an organ! Why we are not there yet. *Prog Polym Sci.* 2019;97:101145.
- Jungst T, Smolan W, Schacht K, et al. Strategies and molecular design criteria for 3D printable hydrogels. *Chem Rev.* 2016;116:1496-1539.
- Dababneh AB, Ozbolat IT. Bioprinting technology: a current state-of-the-art review. *J Manuf Sci Eng.* 2014;136(6):061016.
- Abbott RD, Kaplan DL. Strategies for improving the physiological relevance of human engineered tissues. *Trends Biotechnol.* 2015;33:401-407.
- Matai I, Kaur G, Seyedsalehi A, et al. Progress in 3D bioprinting technology for tissue/organ regenerative engineering. *Biomaterials.* 2020;226:119536.
- Kang D-H, Louis F, Liu H, et al. Engineered whole cut meat-like tissue by the assembly of cell fibers using tendon-gel integrated bioprinting. *Nat Commun.* 2021;12(1):5059.
- Gungor-Ozkerim PS, Inci I, Zhang YS, et al. Bioinks for 3D bioprinting: an overview. *Biomater Sci.* 2018;6:915-946.
- Ng WL, Lee JM, Zhou M, et al. Vat polymerization-based bioprinting—process, materials, applications and regulatory challenges. *Biofabrication.* 2020;12:022001.
- Malda J, Visser J, Melchels FP, et al. 25th Anniversary article: engineering hydrogels for biofabrication. *Adv Mater.* 2013;25:5011-5028.
- Zhang YS, Haghiashtiani G, Hübscher T, et al. 3D extrusion bioprinting. *Nat Rev Methods Primers.* 2021;1:75.
- Ozbolat IT, Hospodiuk M. Current advances and future perspectives in extrusion-based bioprinting. *Biomaterials.* 2016;76:321-343.
- Mandrycky C, Wang Z, Kim K, Kim D-H. 3D bioprinting for engineering complex tissues. *Biotechnol Adv.* 2016;34:422-434.
- Chang CC, Boland ED, Williams SK, Hoying JB. Direct-write bioprinting three-dimensional biohybrid systems for future regenerative therapies. *J Biomed Mater Res B: Appl Biomater.* 2011;98(1):160-170.
- Murphy SV, De Coppi P, Atala A. Opportunities and challenges of translational 3D bioprinting. *Nat Biomed Eng.* 2020;4:370-380.
- Kempner ME, Felder RA. A review of cell culture automation. *JALA: J Assoc Lab Autom.* 2002;7:56-62.
- Schmid FF, Schwarz T, Klos M, et al. Applicability of a dual-arm robotic system for automated downstream analysis of epidermal models. *Appl In Vitro Toxicol.* 2016;2:118-125.
- Leberfinger AN, Dinda S, Wu Y, et al. Bioprinting functional tissues. *Acta Biomater.* 2019;95:32-49.
- Holz K, Lin S, Tytgat L, et al. Bioink properties before, during and after 3D bioprinting. *Biofabrication.* 2016;8:032002.
- Zhang T, Lin S, Shao X, et al. Regulating osteogenesis and adipogenesis in adipose-derived stem cells by controlling underlying substrate stiffness. *J Cell Physiol.* 2018;233:3418-3428.
- Zhang Z, Wu C, Dai C, et al. A multi-axis robot-based bioprinting system supporting natural cell function preservation and cardiac tissue fabrication. *Bioact Mater.* 2022;18:138-150.
- Bunnell BA, Flaata M, Gagliardi C, et al. Adipose-derived stem cells: isolation, expansion and differentiation. *Methods.* 2008;45:115-120.
- Albrecht FB, Dolderer V, Nellinger S, et al. Gellan gum is a suitable biomaterial for manual and bioprinted setup of long-term stable, functional 3D-adipose tissue models. *Gels.* 2022;8(7):420.
- Schmidt FF, Nowakowski S, Kluger PJ. Improvement of a three-layered in vitro skin model for topical application of irritating substances. *Front Bioeng Biotechnol.* 2020;8:388.
- Albrecht FB, Schmidt FF, Volz AC, Kluger PJ. Bioprinting of 3D adipose tissue models using a GelMA-bioink with human mature adipocytes or human adipose-derived stem cells. *Gels.* 2022;8(10):611.
- Das S, Basu B. An overview of hydrogel-based bioinks for 3D bioprinting of soft tissues. *J Indian Inst Sci.* 2019;99:405-428.
- Radtke CP, Hillebrandt N, Hubbuch J. The biomaker: an entry-level bioprinting device for biotechnological applications. *J Chem Technol Biotechnol.* 2018;93:792-799.
- Strauß S, Meutelet R, Radosevic L, et al. Image analysis as PAT-Tool for use in extrusion-based bioprinting. *Bioprinting.* 2021;21:e00112.
- Adhikari J, Roy A, Das A, et al. Effects of processing parameters of 3D bioprinting on the cellular activity of bioinks. *Macromol Biosci.* 2021;21:e2000179.
- Blaeser A, Duarte Campos DF, Puster U, et al. Controlling shear stress in 3d bioprinting is a key factor to balance printing resolution and stem cell integrity. *Adv Healthcare Mater.* 2016;5:326-333.

**How to cite this article:** Albrecht FB, Schmidt FF, Schmidt C, Börret R, Kluger PJ. Robot-based 6D bioprinting for soft tissue biomedical applications. *Eng Life Sci.* 2024;24:e2300226. <https://doi.org/10.1002/elsc.202300226>